Available online at www.sciencedirect.com

SciVerse ScienceDirect

Advances in Space Research 50 (2012) 632–641

ADVANCES IN SPACE RESEARCH (a COSPAR publication)

www.elsevier.com/locate/asr

Effects and disturbances on GPS-derived zenith tropospheric delay during the CONT08 campaign

Haohan Wei [a,b,c], Shuanggen Jin [c], Xiufeng He [a,*]

[a] Institute of Satellite Navigation & Spatial Information System, Hohai University, Nanjing 210098, China
[b] College of Civil Engineering, Nanjing Forestry University, Nanjing 210037, China
[c] Shanghai Astronomical Observatory, Chinese Academy of Sciences, Shanghai 200030, China

Received 28 October 2011; received in revised form 23 March 2012; accepted 22 May 2012
Available online 29 May 2012

Abstract

The zenith total delay (ZTD) can be retrieved from space geodetic techniques, e.g., Global Positioning System (GPS) and Very Long Baseline Interferometry (VLBI), which plays a key role in climatological and atmospheric sciences. However, ZTD estimates still have lots of effects and uncertainties, particularly in GPS model errors. The continuous VLBI observations provide an opportunity to assess GPS ZTD estimates during the Continuous VLBI Campaign 2008 (CONT08) at 11 co-located stations from August 12 to 26, 2008. In this paper, the effects on GPS ZTD estimate and its disturbances are investigated using different mapping function models (GMF, NMF, and VMF1), Phase Center Variation (PCV) models (AZEL and ELEV) and Ocean Tide Loading (OTL) models (FES2004, CSR4.0 and GOT00). It has shown that the ZTDs from VLBI and GPS have an agreement in –3.88–3.74 mm with correlation coefficients of higher than 0.87. For mapping function models, there are no obvious differences, while the PCV model of ELEV is always a little better than AZEL for large scale network with mixed antenna types. For stations near to the coastlines, ocean loading effects must be corrected. While for short period, the effects with OTL models of FFES2004, CSR4.0 and GOT00 are always at the same level. In addition, significant diurnal cycles S_1 (24 h period) and semidiurnal cycles S_2 (12 h period) of GPS ZTD are found with amplitudes between 0.82 and 13.84 mm and 0.30 and 5.23 mm, respectively, which are closer to VLBI ZTD estimates. The correlation coefficients between VLBI and GPS ZTD are 0.85 and 0.95 in S_1 and S_2, respectively.

Keywords: Zenith tropospheric delay; GPS; VLBI; CONT08

1. Introduction

The tropospheric delay is one of the major error sources of space geodetic techniques while their radio signals propagate through the atmosphere, e.g., Global Positioning System (GPS) and Very Long Baseline Interferometry (VLBI). Nowadays the total zenith tropospheric delay (ZTD) can be determined by GPS and VLBI through mapping function (e.g., Niell, 1996; Behrend et al., 2000; Niell et al., 2001; Pacione et al., 2002; Snajdrova et al., 2006), which plays an important role in climatological and atmospheric sciences. The GPS and VLBI-derived ZTDs are the integrated refractivity in the zenith direction, and can be expressed as the sum of the zenith hydrostatic delay (ZHD) related to the surface pressure (Elgered et al., 1991), and the zenith wet delay (ZWD) related to the water vapor (Jin and Luo, 2009).

A number of studies have been carried out on the effects and accuracies of ZTD derived from GPS, VLBI and other ground-based techniques. For example, Behrend et al., 2000 analyzed GPS and VLBI data for 2 weeks in December 1996 at Spain, and found that ZTD differences were smaller than 1 cm. Snajdrova et al. (2006) analyzed continuous VLBI data for 15 days during the Continuous VLBI Campaign 2002 (CONT02) and found that the ZTD differences were about 3 to 10 mm. Meanwhile, a lot of works

* Corresponding author. Tel./fax: +86 25 8378 6310.
E-mail addresses: haohan_wei@sina.com (H. Wei), sgjin@shao.ac.cn (S. Jin), xfhe@hhu.edu.cn (X. He).

0273-1177/$36.00 © 2012 COSPAR. Published by Elsevier Ltd. All rights reserved.
http://dx.doi.org/10.1016/j.asr.2012.05.017

have also demonstrated that VLBI can provide ZTD with high precision and accuracy for meteorological and climatological applications (e.g., Niell et al., 2001; Hatanaka et al., 2001; Heinkelmann et al., 2007). Therefore, the ZTD determined by VLBI can be used as an independent and high-accuracy reference to assess the accuracy and reliability of GPS-estimated ZTD.

Although GPS can provide precise and high temporal resolution ZTD as a highly precise, continuous, all-weather and near-real-time technique, there are lots of effects on GPS ZTD estimates, e.g., mapping functions (Boehm et al., 2007; Won et al., 2010) and Ocean Tide Loading (OTL) models (Vey et al., 2002, 2006; Tregoning and Herring, 2006; Tesmer et al., 2007). For example, Won et al. (2010) analyzed GPS ZTD by testing GMF, NMF, and VMF1 models and found the maximum difference occurred in February and August. Fund et al. (2011) processed 1-year GPS data with different mapping functions, and found significant differences between VMF1 and GMF models due to the GMF's low spatial resolution. Vey et al. (2002) investigated the effects of ocean loading on GPS ZTD and concluded that unmodeled ocean loading has significant effects on GPS ZTD, which must be properly corrected for GPS ZTD estimating. The Continuous VLBI Campaign 2008 (CONT08) was a follow-on campaign of the CONT94, CONT95, CONT96 CONT02 and CONT05 with 11 co-located stations equipping with GPS receivers (Fig. 1). The goal of CONT08 was to acquire state of the art VLBI data over a two-week period (August 12 to 26, 2008) and to provide the highest accuracy of VLBI products, such as the Earth orientation parameters (Nilsson et al., 2010) or tropospheric delay (Teke et al., 2011). Therefore, the independent VLBI provides a unique chance to investigate the reliability and effects of GPS ZTD estimates. In addition, the ZTD has significant diurnal and semidiurnal oscillations, but with a number of possible effects or unknown factors, e.g., ocean tides (Vey et al., 2002) or atmospheric tides (Jin et al., 2008). In this paper, the effects and disturbances on GPS ZTD with different models are investigated, including mapping function models, Phase Center Variation (PCV) models and OTL models. The comparisons between ZTDs derived from VLBI and GPS are performed as well as surface pressure data. A detailed data analysis and post-processing are shown in Section 2. Section 3 presents the results and discussions, including the relations between VLBI/GPS ZTD and altitude, the effects on GPS ZTD and Precipitable Water Vapor (PWV) with different models in GPS data processing, diurnal and semidiurnal cycles of VLBI/GPS ZTD. Finally, conclusions are given in Section 4.

2. Data processing and methods

2.1. VLBI ZTD

The International VLBI Service (IVS) for Geodesy and Astrometry provides the tropospheric products for the IVS-R1 and IVS-R4 sessions, including ZTD estimates of the CONT08 campaigns with 1-h resolution (http://www.dgfi.badw.de/?194). The weighted linear combination of estimates is based on ten IVS Analysis Centers (ACs) using a variance-component estimation approach. The empirical standard deviation of ZTD among the ACs with regard to an unweighted mean is 4.6 mm, and the mean formal error of the unweighted ZTD combination is 2.3 mm (Heinkelmann et al., 2011). Each station of CONT08 is co-located with GPS receiver. Co-located VLBI observations provide an opportunity to assess GPS ZTD estimates during the CONT08 campaign.

2.2. GPS ZTD retrieval

The GAMIT software package was used to estimate the GPS ZTD as a stochastic variation at 1-h sampling from the Saastamoinen model with piecewise linear interpolation in between solution epochs, and a double-difference

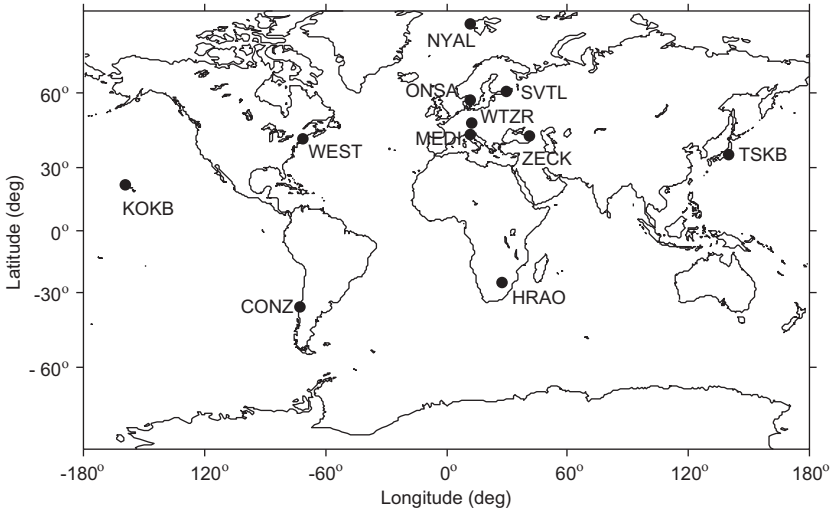

Fig. 1. Distributions of co-located GPS and VLBI stations.

approach was used to solve phase ambiguities, and the percentage of ambiguity success rate is 91.0%–96.4%. Here the International GNSS Service (IGS) Earth orientation parameters and final orbits, International Earth Rotation Service (IERS) solid Earth tide and pole tide model, and an elevation angle cutoff of 7° are used in data processing. In order to investigate the possible effects and diurnal variability of GPS ZTD, different mapping functions (including Global Mapping Function, GMF; Neill Mapping Function, NMF; Vienna Mapping Function 1, VMF1), different PCV models (including elevation-dependent model, ELEV; elevation- and azimuth- dependent model, AZEL), and different OTL models (FES2004, CSR4.0 and GOT00) are used in data processing. So, the ZTD time series from GPS observations at 11 co-located VLBI sites with 1-h resolution are obtained by using different data processing strategies.

3. Results and discussions

3.1. Relations of ZTD and altitude

The ZTD derived from VLBI and GPS is composed of two parts, the hydrostatic part (ZHD) and wet part (ZWD). ZHD accounts for approximately 90% of ZTD, and can be computed as follows (Davis et al., 1985):

$$\mathrm{ZHD} = \frac{2.2768 \pm 0.0005}{1 - 0.00266 \cdot \cos(2\varphi) - 0.00028 \cdot h} \cdot p \approx kp \qquad (1)$$

where φ is the latitude, h is the height (km) above the geoid of the phase center of GPS and VLBI instrument, p is the atmospheric pressure (hPa) at the antenna height, and k is an approximate constant (2.28 mm/hPa). Even in severe weather, the scale factor of k just varies less than 1%. Therefore, the ZHD is proportionate to the atmospheric pressure at the station. In most cases, atmospheric pressure is closely approximated by the hydrostatic pressure caused by the total weight of air above the instrument, so atmospheric pressure is affected by air masses. As we know, with increase of elevation, atmospheric mass decreases. Therefore, atmospheric pressure decreases as altitude increases. The following equation is the approximated relationship between altitude (above the mean sea level) and the atmospheric pressure (http://www.chemistrydaily.com/chemistry/Atmospheric_pressure):

$$\log_{10} p \approx 5 - \frac{h}{15.5} \qquad (2)$$

where p and h are the pressure (Pa) and the altitude (km) above the global mean sea level, respectively. From Eq. (1) and Eq. (2), it can be further deduced as following empirical formula:

$$\mathrm{ZTD} \approx 2.28 \cdot p = 2.28 \cdot 10^{(5-h/15.5)} \cdot 0.01 \qquad (3)$$

where the units of ZTD and h are in millimeters and kilometers, respectively. Fig. 2 shows the distribution of mean GPS ZTD at each co-located station (Table 1). It can be clearly seen that the minimal and maximal values of GPS ZTD are 2.048 m (HRAO, South Africa) and 2.585 m (TSKB, Japan), respectively. Fig. 3 shows the distribution of VLBI/GPS ZTD at all co-located stations and the empirical formula estimates. Blue line, red circle and black triangle stand for the empirical formula estimates, GPS ZTD and VLBI ZTD, respectively. It can be seen that there is a good consistency between VLBI and GPS ZTD and the estimations from the empirical formula. With the altitude increasing, the value of VLBI/GPS ZTD decreases. A little larger differences between VLBI/GPS ZTD and the empirical formula estimates are found below 200 m, which may be due to effects of a large quantity of water vapors in lower atmosphere.

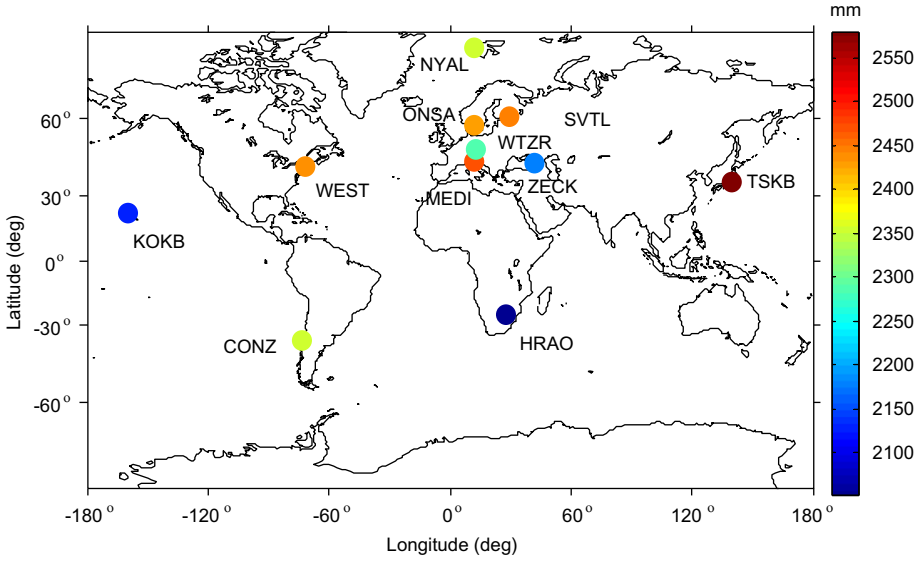

Fig. 2. Distribution of mean GPS ZTD at each co-located station.

Table 1
Comparison of VLBI and GPS ZTD estimates.

Co-located station	GPS receiver type	Lat (deg.)	Lon (deg.)	GPS altitude (m)	VLBI-GPS height difference (m)	VLBI-GPS mean bias (mm)	RMS (mm)	Correlation coefficient
HRAO	ASHTECH UZ-12	−25.89	27.69	1414.1	1.56	−1.45	5.16	0.99
KOKB	ASHTECH UZ-12	22.13	200.33	1167.3	9.24	0.13	7.61	0.95
MEDI	TRIMBLE 4000SSI	44.52	11.65	50.0	17.15	3.74	7.13	0.98
NYAL	AOA BENCHMARK ACT	78.93	11.87	78.6	8.73	3.33	3.07	1.00
SVTL	LEICA SR520	60.53	29.78	76.6	9.36	−0.54	4.70	0.99
TSKB	AOA BENCHMARK ACT	36.10	140.09	67.3	17.44	1.12	9.58	0.99
WTZR	LEICA GRX1200GGPRO	49.15	12.88	666	3.09	0.53	4.50	0.99
ZECK	ASHTECH Z-XII3	43.79	41.57	1166.3	8.71	−0.86	11.44	0.87
CONZ	TPS E_GGD	−36.84	286.97	180.7	−9.73	−2.50	7.86	0.97
WEST	ASHTECH UZ-12	42.61	288.51	85.0	1.77	−3.88	5.50	0.99
ONSA	JPS E_GGD	57.40	11.93	45.6	13.68	2.96	3.98	0.98

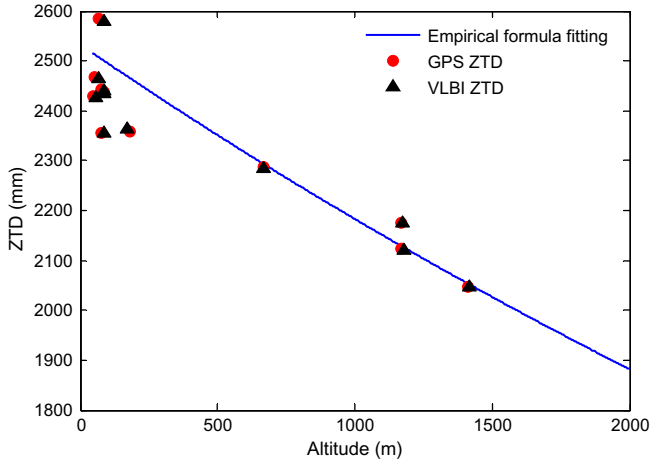

Fig. 3. Distribution of ZTD with altitude (above the global mean sea level). Blue line, red circle and black triangle are empirical formula, GPS ZTD and VLBI ZTD, respectively. (For interpretation of the references to color in this figure legend, the reader is referred to the web version of this article.)

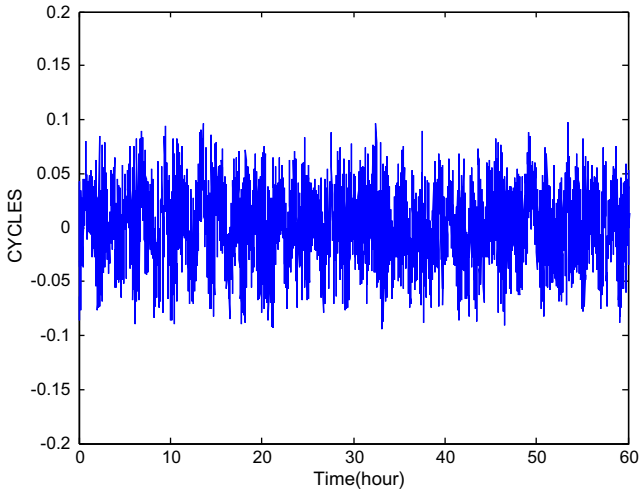

Fig. 4. Double difference residuals (SV Pair: 02-12).

3.2. Comparison of VLBI and GPS ZTDs

In order to check the reliability of GPS ZTD estimates, we compare the ZTDs between VLBI and GPS at all co-located stations during the CONT08 campaign. The mapping function model of GMF, PCV model of ELEV, and OTL model of FES2004 are used to estimate GPS ZTD. Here the influences of different altitudes between VLBI and GPS antennas are corrected. The residuals of double differences show clearly the remaining errors in GPS data processing for ZTD retrieval. Fig. 4 shows the double difference residuals of a pair of satellites in cycles. The mean biases between VLBI and GPS ZTDs at all co-located stations are between −3.88 mm (WEST, USA) to 3.74 mm (MEDI, Italy), with mean-root-square (RMS) from 3.07 mm to 11.44 mm (Table 1), where the correlation coefficients are higher than 0.87 (Fig. 5). The RMS reflects the discrete distributions of ZTD differences. For example, large RMS with 11.44 mm occurred at the station of ZECK (Russia) while the corresponding mean bias is very small (−0.86 mm). It also can be seen in Fig. 5.

3.3. Effects of different models on GPS ZTD estimates

Lots of models affect GPS ZTD estimates. Here different mapping function models, PCV models, and OTL models are investigated and tested in the GPS data processing.

3.3.1. Effects of mapping functions on GPS ZTD estimates

Different mapping function models which have effects on GPS ZTD are investigated and compared with VLBI ZTD, including GMF, NMF, and VMF1, while the PCV model of ELEV and the OTL model of FES2004 are used

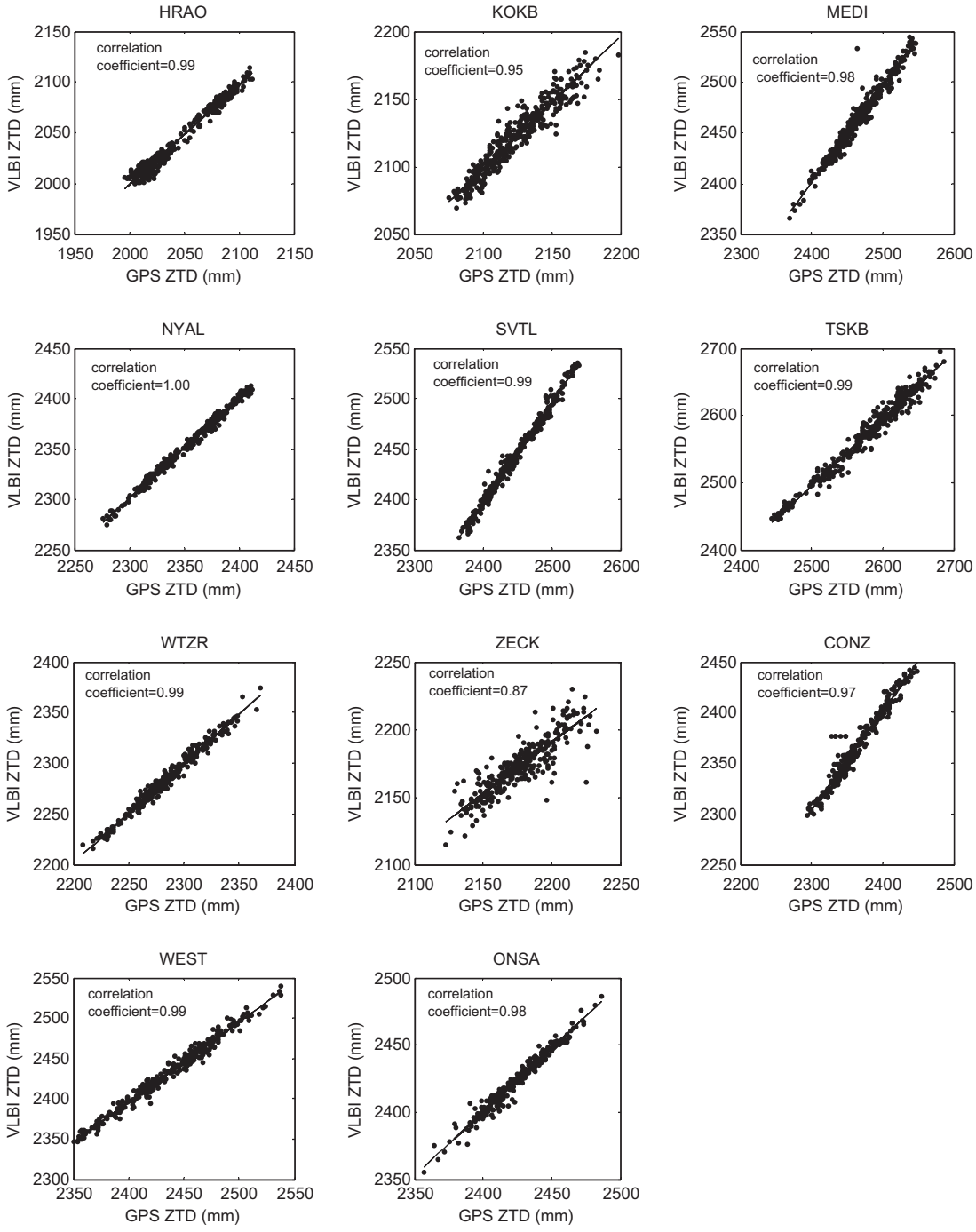

Fig. 5. Correlations between VLBI and GPS ZTDs.

in this case. Fig. 6 shows comparison of GPS ZTD mean differences and RMS using different mapping function models, the left is the mean differences between VLBI/GPS ZTD with different mapping function models. Black bar, gray bar and white bar are estimates with GMF, NMF and VMF1, respectively. The left panel shows that the minimal differences among these models are found at KOKB (USA), ZECK (Russia), and WTZR (Germany), which are all located around 30°N. It has been indicated that there is almost no difference among these mapping function models at the area of around 30°N. Moreover, GPS ZTDs are closer to VLBI ZTDs with VMF1 model than those with the other two models at NYAL (Norway), which indicates that in the area of high latitude of the Northern Hemisphere, VMF1 model can introduce more precise GPS ZTD then other models. Besides, the effects of NMF model are a little larger than the other two models at CONZ (Chile) and TSKB (Japan). These agree with Boehm's results that in high southern latitudes and in Japan, NMF model always has apparent biases (Boehm

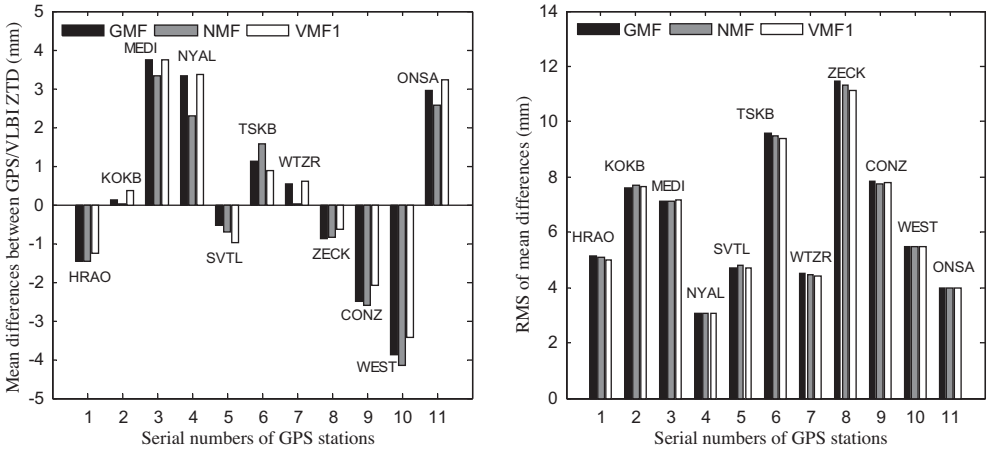

Fig. 6. Mean differences and root mean squares (RMS) between VLBI and GPS ZTD with different mapping function models. Black bar, gray bar and white bar illustrate mean differences with GMF, NMF and VMF1, respectively.

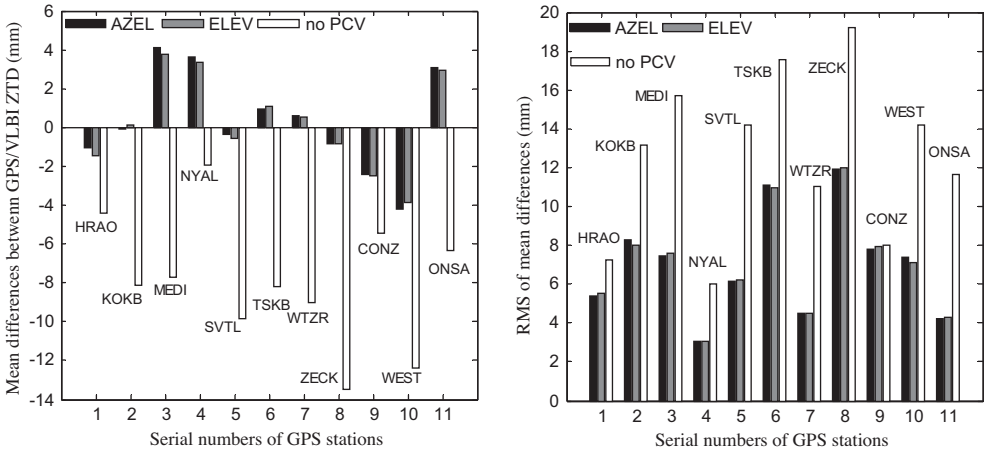

Fig. 7. Mean differences and RMS between VLBI and GPS ZTD with different PCV models while mapping function model of GMF. Black bar, gray bar and white bar are mean differences with AZEL, ELEV, and without any PCV model, respectively.

et al., 2006). Moreover, GMF and VMF1 models both have almost the same effects on GPS ZTD in the other areas of the world. The right panel of Fig. 6 shows the RMSs of the differences between VLBI and GPS ZTD with these three models. It can be seen that in general, the accuracies of the three mapping functions are always at the same level, which may be due to the short period of the CONT08 campaign. In addition, using the PCV model of AZEL, similar results are obtained with different mapping function models.

3.3.2. Effects of PCV on GPS ZTD estimates

Different PCV models are used for GPS ZTD estimates, which are compared with VLBI ZTD, including ELEV and AZEL models. Here the mapping function model of GMF and the OTL model of FES2004 are used in this case. Fig. 7 shows the effects on GPS ZTD estimates with different PCV models. The left panel is the mean differences between VLBI and GPS ZTD with different PCV models. Black, gray, and white bars denote the mean differences with AZEL, ELEV, and without PCV model, respectively. The significantly negative systematic differences of VLBI minus GPS ZTD are found from −1.93 mm (NYAL, Norway) to −13.47 mm (ZECK, Russia) without using any PCV model. When PCV models are used, the differences between VLBI and GPS ZTD are greatly reduced, indicating that the GPS antenna model must be used in GPS data processing. While the mean differences using the ELEV model are a little better than the AZEL model, excluding the stations HRAO (South Africa), SVTL (Russia), and TSKB (Japan). It may be the fact that the ELEV model is important for large scale network with mixed antenna types (see Table 1) (Herring et al., 2006). The RMSs of mean differences with ELEV and AZEL models are almost similar, seeing the right panel of Fig. 7. In addition, using the mapping function model of VMF1, similar results are obtained from the effects on GPS ZTD estimates with different PCV models (see Fig. 8).

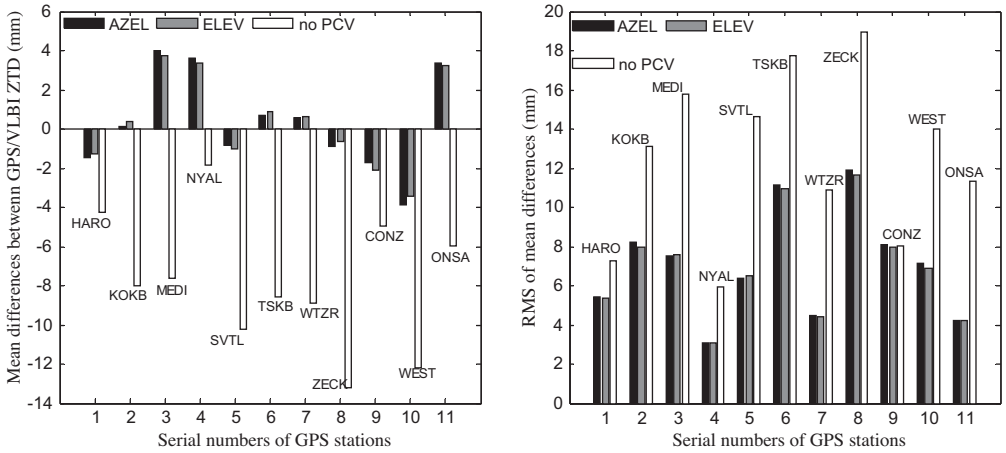

Fig. 8. Mean differences and RMS between VLBI and GPS ZTD with different PCV models while mapping function model of VMF1. Black bar, gray bar and white bar are mean differences with AZEL, ELEV, and without any PCV model, respectively.

Table 2
RMS and correlation coefficients between VLBI and GPS ZTD with OTL model of FES2004, CSR4.0, GOT00, and without OTL model.

Co-located station	RMS (mm)				Correlation coefficients			
	FES2004	CSR4.0	GOT00	NO OTL	FES2004	CSR4.0	GOT00	NO OTL
HRAO	5.0619	5.5823	5.2148	5.6257	0.9885	0.9858	0.9876	0.9858
KOKB	7.8521	7.5907	7.6432	8.7665	0.9541	0.9571	0.9565	0.9424
MEDI	7.1289	7.1270	7.1538	7.1566	0.9800	0.9800	0.9799	0.9797
NYAL	3.0376	3.0783	3.0333	3.3629	0.9958	0.9957	0.9959	0.9949
SVTL	4.6807	4.6976	4.6721	4.7509	0.9933	0.9933	0.9934	0.9932
TSKB	9.5521	9.5207	9.4718	9.7979	0.9852	0.9853	0.9854	0.9845
WTZR	4.4364	4.4802	4.4512	4.5190	0.9892	0.9888	0.9890	0.9887
ZECK	11.3300	11.3170	11.2760	11.2340	0.8708	0.8707	0.8726	0.8745
CONZ	7.8691	7.9947	7.9053	7.9564	0.9740	0.9734	0.9739	0.9739
WEST	5.4572	5.5073	5.4636	5.9008	0.9903	0.9901	0.9903	0.9887
ONSA	4.0130	3.9697	4.0252	4.0685	0.9832	0.9835	0.9830	0.9821

3.3.3. Effects of OTL models on GPS ZTD estimates

Different OTL models are used in GPS data processing, including CSR4.0, GOT00 and FES2004 models. The mapping function model of VMF1 and PCV model of AZEL are used in this case. Table 2 shows the RMS and correlation coefficients between VLBI and GPS ZTD with different OTL models and without OTL model. It indicates that if any OTL model used, the RMS of ZTD differences are always better than those without OTL model, except for the stations of ZECK (Russia) which is located in the mainland of Europe, and CONZ (Chile) which is located in the Southern Hemisphere. The former (ZECK) has little ocean loading effects on GPS ZTD since the station is far from the ocean. To verify and compare the ocean loading effects on the station of CONZ and on other stations, vertical displacements derived from FES2004 model are provided by Fig. 9. It can be seen clearly that due to little effects on vertical direction derived from OTL model(less than 10 mm), there's no significant difference between GPS ZTD with and without OTL model at the station of CONZ. Moreover, Table 2 shows that there's no apparent difference between these OTL models of FES2004, GOT00 and CSR4.0.

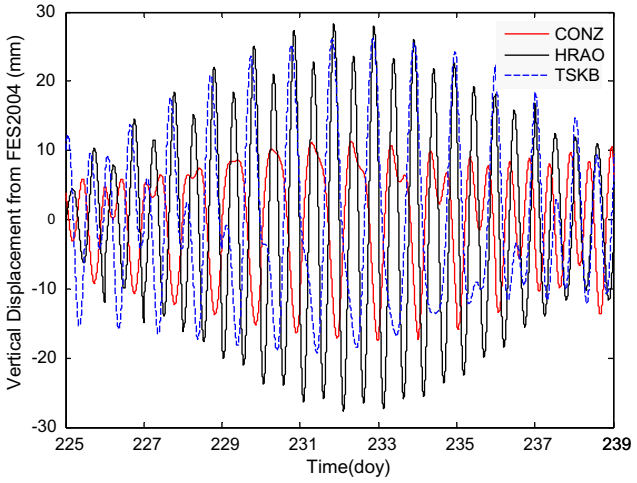

Fig. 9. Vertical site displacements (in mm) derived from FES2004 model at the stations of CONZ, HRAO, and TSKB during CONT08. Red, black and blue lines are vertical displacements at the stations of CONZ, HRAO and TSKB, respectively. (For interpretation of the references to colour in this figure legend, the reader is referred to the web version of this article.)

As the ocean tide effects are most at diurnal time scales, the mean diurnal variations of each ZTD time series are

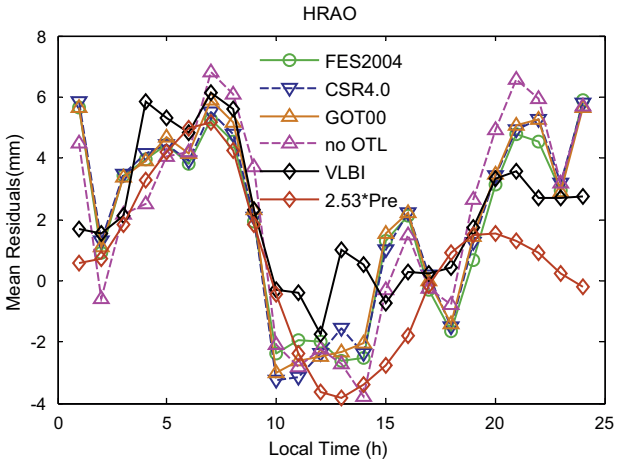

Fig. 10. Diurnal cycles of GPS ZTD (with different OTL models), VLBI ZTD and surface pressure at HRAO, South Africa. Green, blue, brown and purple lines are mean residuals of GPS ZTD with OTL models of FES2004, CSR4.0, GOT00, and without any OTL model, respectively. Black and red lines are VLBI ZTD and ZTD deduced from surface pressure, respectively. (For interpretation of the references to colour in this figure legend, the reader is referred to the web version of this article.)

investigated at all co-located sites. It also shows inconspicuous differences between the three OTL models. For example, Fig. 10 shows diurnal ZTD variations at the co-located station HRAO (South Africa). Green, blue, brown and purple lines are mean residuals of diurnal GPS ZTD using OTL models of FES2004, CSR4.0, GOT00, and without OTL model, respectively. Black and red lines are VLBI ZTD and ZTD deduced from surface pressure, respectively. Moreover, the ZTD derived from surface pressure has a good consistency with VLBI ZTD, with correlation coefficient of 0.88.

3.4. Diurnal and semidiurnal cycles of ZTD

The VLBI/GPS ZTD time series of each station are analyzed using the Fast Fourier Transform. Here the mapping function model of GMF, PCV model of ELEV, and OTL model of FES2004 are used to estimate GPS ZTD. Strong signals at about 12-hour and 24-hour of VLBI/GPS ZTDs are found, indicating significant diurnal cycles S_1 (24 h period) and semidiurnal cycles S_2 (12h period) in VLBI/GPS ZTD time series. For example, Fig. 11 shows the original VLBI/GPS ZTD time series (upper) and power spectrum (bottom) with one hour interval at the co-located station TSKB. In order to find the diurnal (S_1) and semidiurnal (S_2) variations of ZTD time series derived from GPS and VLBI during the 15 days of the CONT08 campaign, the following harmonic function has been used:

$$\mathrm{ZTD}_t = a + \sum_{i=1}^{2}[S_i \sin(2\pi(t - t_0)/p_i + \varphi_i)] + \varepsilon_t \quad (4)$$

where t is the time (hours), a is the constant term, S_i, p_i, ϕ_i are the amplitude, period, and phase at period i, respectively, and ε_t is the residual. Using the least square method, the amplitudes of S_1, S_2 and their uncertainties of the VLBI/GPS ZTD series are determined (see Table 3). The amplitudes of S_1 and S_2 of GPS ZTD are 0.82–13.84 mm and 0.30–5.23 mm, respectively, which are closely to those

Table 3
Diurnal (S_1) and semidiurnal (S_2) amplitude of VLBI/GPS ZTD.

Co-located station	GPS ZTD (mm)		VLBI ZTD (mm)	
	S1	S2	S1	S2
HRAO	2.72±0.24	1.24±0.53	2.01±0.30	1.62±0.37
KOKB	5.24±0.26	2.50±0.55	7.58±0.18	2.83±0.48
MEDI	3.64±0.49	2.39±0.75	3.21±0.55	1.57±1.13
NYAL	0.82±0.72	0.30±2.01	1.37±0.45	0.25±2.49
SVTL	6.95±0.21	0.52±2.72	7.12±0.19	2.11±0.65
TSKB	7.46±0.22	5.23±0.32	5.72±0.31	4.94±0.36
WTZR	4.22±0.31	1.74±0.75	2.42±0.32	1.13±0.71
ZECK	13.84±0.12	2.33±0.73	13.53±0.11	2.14±0.69
CONZ	4.35±0.26	0.68±1.69	4.48±0.23	0.39±2.60
WEST	3.73±0.46	2.79±0.61	3.01±0.57	1.50±1.14
ONSA	1.43±0.81	0.93±1.25	1.48±0.76	1.03±1.10

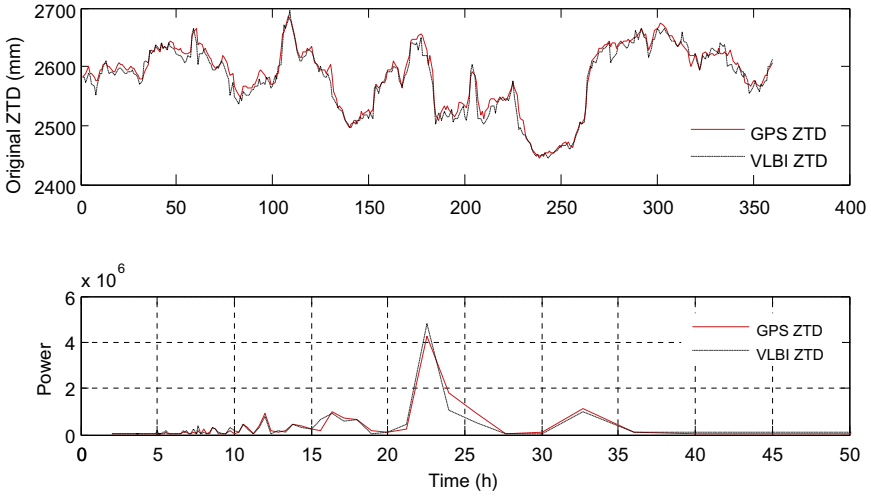

Fig. 11. Time series of VLBI/GPS ZTD (upper) and power spectrum (bottom) at TSKB (Japan).

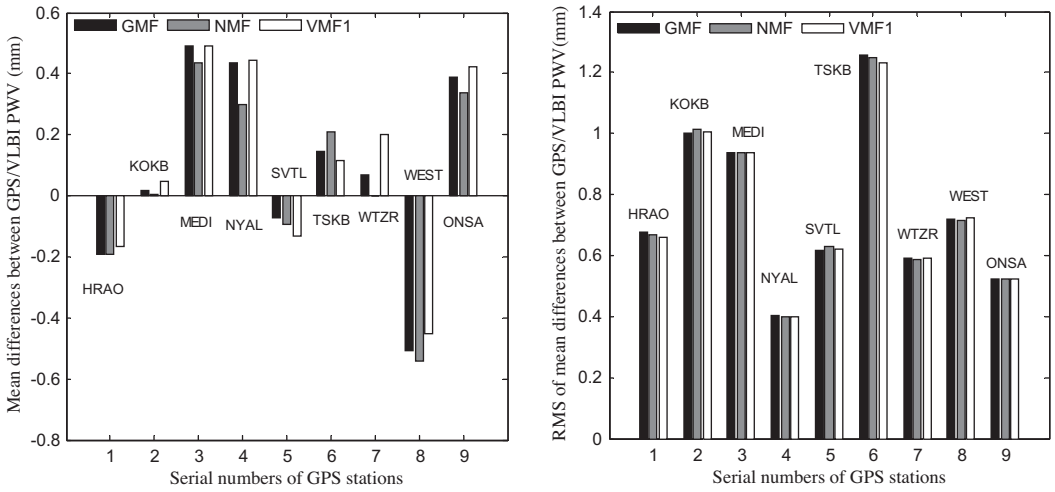

Fig. 12. Mean differences and RMS between VLBI/GPS PWV with different mapping functions. Black bar, gray bar and white bar are mean differences with GMF, NMF and VMF1, respectively.

of VLBI ZTD with correlation coefficients of 0.95 and 0.85, respectively.

3.5. Effects of different models on GPS PWV estimates

The retrieval of PWV from GPS ZTD is very important for GPS meteorological applications. The PWV is defined as the total atmospheric water vapor contained in a vertical column above the station, which can be derived from ZWD as follows (Bevis et al., 1994):

$$\mathrm{PWV} = \prod \times \mathrm{ZWD} \tag{5}$$

where

$$\prod = \frac{10^6}{\rho R_v[(k_3/T_m + k_2')]} \tag{6}$$

where ρ is the density of liquid water, R_v is the specific gas constant for water vapor, k_3 and k_2' are physical constants and T_m is the mean temperature of the atmosphere, which can be computed from surface temperature as $T_m = 70.2 + 0.72T_S$ (Bevis et al., 1992). In this study, the surface temperature is observed at each co-located station except for the stations of CONZ and ZECK. In order to investigate the effects of different models on GPS PWV estimates, different mapping functions, OTL models, and PCV models are used to test as comparing with VLBI PWV. Fig. 12 shows the mean differences and RMSs between VLBI/GPS PWV with different mapping functions. it can be seen that the mean differences are all less than 0.5 mm, and RMSs are not more than 1.3 mm, indicating that the effects of different mapping functions on GPS PWV estimates are very small, which can be ignored. For OTL models and PCV models, there are no obvious different effects on GPS PWVs.

4. Conclusions

The effects and variations of GPS ZTD estimates with 1 hour resolution are investigated and compared with VLBI ZTD at 11 co-located stations during the CONT08 campaign. It has been shown that at the area about 30°N, there are no obvious differences among GPS ZTDs with different mapping functions of GMF, NMF, and VMF1. For PCV model, the ELEV model is more important for large scale network with mixed antenna types. Meanwhile, for stations near to the coastlines, ocean loading effects must be corrected for GPS ZTD retrieval, except for station of CONZ (Chile), where the effect from ocean loading is smaller. And the effects on GPS ZTD from OTL models of FES2004, CSR4.0, and GOT00 are almost at the same level in short period. Moreover, comparison of VLBI and GPS ZTD shows that they have a good agreement in −3.88–3.74 mm with correlation coefficients of higher than 0.87. Also significant signals of VLBI/GPS ZTD time series at about 12 and 24 h are found, and their diurnal (S_1) and semidiurnal (S_2) amplitudes of ZTD have a good agreement. In addition, the effects on GPS PWV estimates are relatively small with different mapping functions, OTL models and PCV models. Although the CONT08 campaign provides a good opportunity to evaluate the effects on GPS ZTD estimates with different models, the continuous observation time is short with just 15 days and the number of co-located stations is a few with just eleven sites. Longer period and more co-located sites for further investigation are expected in the near future.

Acknowledgements

We thank the data and products provided by the International VLBI Service for Geodesy and Astrometry (IVS) and the International GNSS Service (IGS). This work was supported by the National Basic Research Program of China (973 Program) (Grant No. 2012CB720000), Main Direction Project of Chinese Academy of Sciences (Grant No. KJCX2- EW-T03), Shanghai Pujiang Talents Program Project (Grant No. 11PJ1411500) and Surveying and Mapping Projects of Jiangsu Province (Grant No. JSCHKY201214).

References

Behrend, D., Cucurull, L., Vila, J., Haas, R. An inter-comparison study to estimate zenith wet delays using VLBI, GPS and NWP models. Earth Planets Space 52, 691–694, 2000.

Bevis, M., Businger, S., Herring, T.A., Rocken, C. GPS meteorology: Remote sensing of atmospheric water vapor using the global positioning system. J. Geophys. Res. 97 (15), 15,787–15,801, 1992.

Bevis, M., Businger, S., Chiswell, S., Herring, T.A., Anthes, R.A., Rocken, C., et al. GPS meteorology: mapping zenith wet delays onto precipitable water. J. Appl. Met. 33, 379–386, 1994.

Boehm, J., Niell, A., Tregoning, P., Schuh, H. Global mapping function (GMF): a new empirical mapping function based on numerical weather model data. Geophys. Res. 33, L07304, 1–4, 2006.

Boehm, J., Mendes, C.P.J., Schuh, H., Tregoning, P. The impact of tropospheric mapping functions based on numerical weather models on the determination of geodetic parameters. In: Tregoning, P., Rizos, C. (eds), Dynamic planet—monitoring and understanding a dynamic planet with geodetic and oceanographic tools. Springer, International Association of Geodesy Symposia, vol. 130, pp. 837–843, 2007.

Davis, J.L., Herring, T.A., Shapiro, I.I., Rogers, A.E.E., Elgered, G. Geodesy by radio interferometry: effects of atmospheric modelling errors on estimates of baseline length. Radio Sci. 20 (6), 1593–1607, 1985.

Elgered, G., Davis, J.L., Herring, T.A., Shapiro, I.I. Geodesy by radio interferometry: water vapor radiometry for estimation of the wet delay. J. Geophys. Res. 95 (B4), 6541–6555, 1991.

Fund, F., Morel, L., Mocquet, A., Boehm, J. Assessment of ECMWF-derived tropospheric delay models within the EUREF Permanent Network. GPS Solut. 15, 39–48, 2011.

Hatanaka, Y., Sawada, M., Horita, A., Kusaka, M. Calibration of antenna-radome and monument-multipath effect of GEONET, part 1, measurement of phase characteristics. Earth Planets Space 53 (1), 13–21, 2001.

Heinkelmann, R., Boehm, J., Schuh, H., Bolotin, S., Engelhardt, G., MacMillan, D.S., Negusini, M., Skurikhina, E., Tesmer, V., Titov, O. Combination of long time-series of troposphere zenith delays observed by VLBI. J. Geod. 81, 483–501, 2007. Available from: <http://www.springerlink.com/content/b2720k4081136211/>.

Heinkelmann, R., Böhm, J., Bolotin, S., Engelhardt, G., Hass, R., Lanotte, R., MacMillan, D.S., Negusini, M., Skurikhina, E., Titov, O., et al. VLBI-derived troposphere parameters during CONT08. J. Geod. 85, 377–393, 2011.

Herring, T.A., King, R.W., McClusky, S.C. GAMIT Reference Manual: GPS Analysis at MIT. Dep. of Earth, Atmos., and Planet. Sci., Mass. Inst. of Technol, Cambridge, Release 10.3, pp. 47–48, 2006.

Jin, S.G., Luo, O. Variability and climatology of PWV from global 13-year GPS observations. IEEE Trans. Geosci. Remote Sens. 47 (7), 1918–1924, 2009.

Jin, S.G., Wu, Y., Heinkelmann, R., Park, J. Diurnal and semidiurnal atmosperic tides observed by co-located GPS and VLBI measurements. J. Atmos. Solar-Terrest. Phys. 70, 1366–1372, 2008.

Niell, A.E. Global mapping functions for the atmosphere delay at radio wavelengths. J. Geophys. Res. 101 (B2), 3227–3246, 1996.

Niell, A., Coster, A., Solheim, F., Menders, V., Toor, P., Langley, R., Upham, C. Comparison of measurements of atmospheric wet delay by radiosonde, water vapor radiometer, GPS, and VLBI. J. Atmos. Oceanic Technol. 18 (6), 830–850, 2001.

Nilsson, T., Böhm, J., Schuh, H. Sub-diurnal earth rotation variations observed by VLBI. Artif. Sat. 45 (2), 49–55, 2010.

Pacione, R., Fionda, E., Ferrara, R., Lanotte, R., Sciarretta, C., Vespe, F. Comparison of atmospheric parameters derived from GPS, VLBI and a ground-based microwave radiometer in Italy. Phys. Chem. Earth. 27, 309–316, 2002.

Snajdrova, K., Boehm, J., Willis, P., Haas, R., Schuh, H. Multi-technique comparison of tropospheric zenith delays derived during the CONT02 campaign. J. Geod. 79, 613–623, 2006.

Teke, K., Böhm, J., Nilsson, T., et al. Multi-technique comparison of troposphere zenith delays and gradients during CONT08. J. Geod. 85, 395–413, 2011.

Tesmer, V., Boehm, J., Heinkelmann, R., Schuh, H. Effect of different tropospheric mapping functions on the TRF, CRF and position time-series estimated from VLBI. J. Geod. 81, 409–421, 2007.

Tregoning, P., Herring, T.A. Impact of a priori zenith hydrostatic delay errors on GPS estimates of station heights and zenith total delays. Geophys. Res. Lett. 33, L01814, 1–5, 2006.

Vey, S., Calais, E., Llubes, M., et al. GPS measurements of ocean loading and its impact on zenith tropospheric delay estimates: a case study in Brittany. France J. Geod. 76, 419–427, 2002.

Vey, S., Dietrich, R., Fritsche, M., Rülke, A., Rothacher, M., Steigenberger, P. Influence of mapping function parameters on global GPS network analyses: comparisons between NMF and IMF. Geophys. Res. Lett. 33, L01814, 1–4, 2006.

Won, J., Park, K., Ha, J., Cho, J. Effects of tropospheric mapping functions on GPS data processing. J. Astron. Space Sci. 27, 21–30, http://www.chemistrydaily.com/chemistry/Atmospheric_pressure, 2010.